

Article

Tribological Properties and Corrosion Resistance of Multilayer a-C:H:Ti Films at Different Target Currents

Yaqi Huang^{1,2,3}, Jia Li^{1,3,*}, Xuhui Wang^{1,2,3}, Xiaohong Liu², Hongxuan Li², Pengwei Ren^{2,*} and Chufeng Sun^{1,3}

¹ School of Chemical Engineering, Northwest Minzu University, Lanzhou 730000, China; y211830597@stu.xbmu.edu.cn (Y.H.); y211830616@stu.xbmu.edu.cn (X.W.); chufengsun@xbmu.edu.cn (C.S.)

² State Key Laboratory of Solid Lubrication, Lanzhou Institute of Chemical Physics, Chinese Academy of Sciences, Lanzhou 730000, China; xhliu@licp.cas.cn (X.L.); lihx@licp.cas.cn (H.L.)

³ Key Laboratory of Environment-Friendly Composite Materials, the State Ethnic Affairs Commission, Gansu Provincial Biomass Function Composites Engineering Research Center, Key Laboratory for Utility of Environment-Friendly Composite Materials and Biomass, University of Gansu Province, Lanzhou 730030, China

* Correspondence: lj5458325@126.com (J.L.); renpengwei@licp.cas.cn (P.R.)

Abstract: To meet the requirements of friction and corrosion resistance performance of helicopter transmission bearings under harsh environments, Ti/TiN/Ti-DLC multilayer composite films were prepared on a 40Cr15Mo2VN substrate by a non-equilibrium magnetron sputtering technique. The effects of different titanium currents on the structure, mechanical properties, and friction properties of the films were investigated by SEM, Raman spectroscopy, and nanoindentation. Moreover, the tribological and corrosion resistance of developed films under acidic conditions were investigated. The results show that the sp^3 -C/ sp^2 -C ratio in the films gradually decreases with increasing Ti current from 0 A to 2 A, leading to decreased hardness and elastic modulus. The bonding force of the DLC films also gradually increases with increasing Ti current and reaches the maximum value of 41.69 N at 2 A; the friction coefficient of the films gradually decreases under a load of 20 N. In summary, the best performance of thin film at Ti-2 A was compared with the corrosion and wear performance of thin film and substrate in acetic acid solution and aqueous solution at Ti-2 A. The wear amount of thin film and substrate in aqueous solution is significantly lower than in acetic acid solution, and the corrosion potential of thin film is higher than that of substrate in both solutions, which can play a protective role against the substrate.

Keywords: Diamond-Like Carbon film; corrosion and wear; titanium target current; unbalanced magnetron sputtering



Citation: Huang, Y.; Li, J.; Wang, X.; Liu, X.; Li, H.; Ren, P.; Sun, C.

Tribological Properties and Corrosion Resistance of Multilayer a-C:H:Ti Films at Different Target Currents.

Metals **2023**, *13*, 1274. <https://doi.org/10.3390/met13071274>

Academic Editor: Petros E. Tsakiridis

Received: 5 June 2023

Revised: 2 July 2023

Accepted: 4 July 2023

Published: 15 July 2023



Copyright: © 2023 by the authors. Licensee MDPI, Basel, Switzerland. This article is an open access article distributed under the terms and conditions of the Creative Commons Attribution (CC BY) license (<https://creativecommons.org/licenses/by/4.0/>).

1. Introduction

High-nitrogen steel with high mechanical properties is widely used in the fabrication of shafts, gears, and bearings in various industrial fields. However, in corrosive environments, it suffers interrelated tribocorrosion damage. Mechanical wear and electrochemical corrosion generally accelerate each other, and the most effective protection method has been the subject of academic and engineering interest.

Diamond-Like Carbon (DLC) is a solid lubricant containing a sp^3 and sp^2 hybridized carbon structure that has been widely used in mechanical, electronic, and biomedical fields due to its high hardness, excellent anti-friction properties, and corrosion resistance. In 1971, an amorphous carbon film with physical and chemical properties close to those of diamond was successfully prepared for the first time and was called Diamond-Like Carbon film. DLC films have a high hardness and high modulus of elasticity, especially those prepared by laser sputtering or the magnetic filtering cathodic arc method, with a hardness of 70–110 GPa, which is comparable to that of diamond. In addition to high hardness, DLC films usually have high internal stress, which not only limits the film thickness but also

severely affects the bond strength, service life, and tribological properties of the film. This internal stress can lead to cohesion and bond cracking and rupture of the coating during its service life, especially at high load values, which can lead to an increase in the wear rate and friction coefficient. In response to this problem, some experts have proposed solutions such as adding elements, introducing transition layers, and constructing multilayer films, which to some extent improve the bond strength between the film and the substrate, thus increasing the load-bearing capacity of thick films.

Sun et al. [1] reviewed the effects of doping of carbide-forming elements and non-carbide-forming elements on the properties of DLC films, and the appropriate amount of elemental doping can significantly reduce the residual stress of the films, improve the bonding between the films and the substrate, and improve the tribological, hydrophobic, corrosion resistance, and antibacterial properties of the films without significantly reducing the mechanical properties of the films, which broadens the application areas. The addition of Si to DLC coatings reduces the stress in amorphous hydrogenated carbon films. Dorota Bociaga et al. [2] showed that with the addition of Si, the disorder of the films increases, likely due to the formation of sp^3 -C. The doping of Si significantly improved the wear properties and resistance to plastic deformation of the films. Second, the content of doped elements also affects the mechanical properties of the films, but in general, the properties of the element-doped films are superior to those of the undoped films. Rajesh et al. [3] prepared copper-alumina composites and investigated the corrosion and wear behavior of copper metal matrix composites reinforced with different weight percentages (5, 10, and 15%) of alumina, and obtained the best wear performance and corrosion resistance at 15% and 10% alumina content, respectively. Jing et al. [4] deposited silver (Ag)-doped diamond-like films (Ag-DLC) on Si wafers and Co-Cr-Mo alloy substrates using a hybrid deposition technique combining high-power pulsed magnetron sputtering (HPPMS) and high-power pulsed plasma-enhanced chemical vapor deposition (HPP-PECVD). The results show that Ag doping can refine the columnar structure in DLC films, change the shape and size of DLC surface mounds, and effectively improve the bonding between films and substrates. Zhu et al. [5] deposited Cr-doped DLC films on the surfaces of stainless steel and silicon wafers using a nonequilibrium magnetron sputtering deposition technique. The doped elements are inhomogeneously distributed in the three-dimensional network structure of amorphous carbon, forming a multicomponent composite structure of nanocrystals and amorphous states. The nanocrystals can effectively reduce the internal stress and improve the toughness of the films. For the film base bonding problem, Zhang et al. deposited H-DLC films on the surface of a 13Cr substrate using a high pulse power CVD method, and the film base bonding reached 61 N [6]. Liu et al. reduced the internal stress of the films by introducing a TiAlN transition layer, and the film base bonding reached 63 N [7]. Javidparvar et al. [8] doped copper in DLC-based coatings on nickel-bronze aluminum alloy (NiBrAl), and electrochemical analysis showed that the corrosion resistance of pure DLC coatings improved nearly three times compared with that of the substrate. Su et al. [9] prepared Mo-doped DLC films using magnetron sputtering equipment and found that Mo doping moderated the internal stress of the DLC films and improved the adhesion of the DLC films. Zhang et al. investigated the effect of Ti target current on the properties of Ti-DLC films and showed that the wear rate and friction coefficient of the films were lower when a low Ti current was deposited. Meanwhile, the addition of Ti improved its corrosion resistance [10]. Li et al. [11] found that the optimized Cr/GLC multilayer interface can effectively hinder the formation of penetration defects, reduce the generation of corrosion channels, inhibit the penetration of corrosion ions, and significantly enhance the corrosion resistance of the film. Fayed et al. [12] formed multilayer DLC-Si films on aluminum alloy by the ionophore-enhanced chemical vapor deposition (PECVD) technique. The multilayer film introduced a new interface that prevented the penetration of Cl^- ions. Song et al. [13] designed a novel multilayer coating containing a two-phase structure by magnetron sputtering, and the multilayer coating significantly improved its corrosion resistance. Ye et al. [14] successfully prepared multilayer DLC coatings on the surface

of 304 L stainless steel and silicon wafers using a non-equilibrium magnetron sputtering method and investigated the corrosion and wear behavior of the coatings and the substrate materials in seawater. The results show that the friction coefficient of the coated samples decreases and the wear loss increases as the polarization potential rises from -1 V to 0.5 V. In addition, the mechanical wear of 304 L substrate decreased significantly with increasing polarization potential, and corrosion-induced wear gradually dominated, but the main volume loss of multilayer DLC coatings was mainly due to pure mechanical wear. Therefore, the multilayer DLC coating has better corrosion and wear resistance than the 304 L substrate in seawater and provides good protection.

Therefore, doping elements, generating transition layers, and designing gradient layers/multilayers can improve the mechanical properties of the films, reduce the residual stresses in films, and improve the bonding and corrosion resistance of substrates and the films. Ti is a preferred choice as a doping element for DLC films because of its ability to improve the frictional properties, thermal stability, and adhesive strength of the films. Ti doping accelerates graphitization under the catalytic effect of frictional heating. However, the corrosion and wear behavior of DLC and its protection effect on high-nitrogen steel bearing materials in corrosive media remain unclear, which limits its engineering applications.

In this paper, Ti/TiN/Ti-DLC films with different Ti contents were prepared on a high-nitrogen steel (40Cr15Mo2VN) substrate by a non-equilibrium magnetron sputtering technique, and the sputtering current of the Ti target was varied to control the Ti doping content. The effects of different Ti contents on the film composition, structure, mechanical properties, and tribological properties, as well as the corrosion and wear properties of the films and substrates in an acetic acid solution with a pH value of 3, were investigated.

2. Experiment

2.1. Coating System

The test coating equipment used is the high-power ion density lubrication deposition system (CF-800, Teer, London, Britain), which is equipped with four magnetron sputtering targets (two carbon targets and two titanium targets), biased by pulsed DC, and the target current is supplied DC. In this device, the magnetic fields of adjacent magnetron targets are of opposite polarity, with magnetic lines of force emanating from the N-pole of one target and mostly close to the S-pole of the adjacent target. This system creates a high ion flow at the substrate that is significantly higher than that of a single unbalanced magnetron sputtering target device. This closed-field, nonequilibrium magnetron sputtering system is very effective for the uniform deposition of complex substrates. Currently, closed-field nonequilibrium magnetron sputtering technology is widely used in the production of superhard and self-lubricating films on cutting tools, coated glass for architectural and automotive applications, and transparent conductive glass for the electronics industry.

The technical advantage of nonequilibrium magnetron sputtering is that low-energy, high-density bombardment ions are used in the deposition coating process. The structure of the prepared layer is dense, and the internal stress in the layer is very low. The deposition temperature is low during the preparation of the film layer, and the impact on the substrate is minimal. Highly efficient ion cleaning results in high bonding between film layer and substrate, making it easy to deposit excellent multilayer film layers. Fully automated computer operation allows preparation of various desired film layers.

2.2. Film Preparation

The DLC films were prepared using a closed-field unbalanced magnetron sputtering device (CF-800, Teer, Birmingham, UK), equipped with four magnetron sputtering targets (two carbon targets and two titanium targets). Before preparing the films, the substrate silicon wafers and 718 steel blocks were ultrasonically cleaned in deionized water and acetone, respectively, and then dried to remove surface contaminants, after which they were deposited in the deposition chamber. The process parameters for film deposition are shown in Table 1. The deposition process is divided into four steps: (1) pump the coating

chamber to vacuum, pass argon gas, and adjust the substrate bias for argon ion etching to remove the contaminants on the substrate surface; (2) adjust the titanium target current and deposit the titanium primer layer; (3) adjust the carbon target and titanium target current and pass nitrogen gas to deposit the titanium nitride transition layer; and (4) pass methane gas to adjust the titanium target current and keep the carbon target sputtering current at 5 A to deposit titanium doped with different titanium hydrogen-containing carbon films with different titanium contents.

Table 1. Process parameters for the DLC film preparation.

Samples	Ti Target Current (A)	Bias Voltage (V)	CH ₄ /Ar (sccm)	C Target Current (A)
Ti-0 A	0			
Ti-0.5 A	0.5			
Ti-1.0 A	1.0	−200	40/30	5
Ti-1.5 A	1.5			
Ti-2.0 A	2.0			

2.3. Performance Characterization

The cross-sectional morphology of the films was characterized by ultra-high resolution field emission scanning electron microscopy (SU8020, Hitachi, Tokyo, Japan), and the surface morphology of the films was observed by field emission scanning electron microscopy (Quanta 650 FEG, FEI, Hillsboro, OH, USA). The film base bonding of the carbon films was characterized by a REVETEST scratch meter (RST, CSM, Basel, Switzerland) with a loading load range of 0–100 N, a scratch length of 5 mm, and a loading rate of 50 N/min for each sample repeated three times. The original surfaces of the coatings were analyzed by Raman spectroscopy (LabRAM HR Evolution, HORIBA JobinYvon S.A.S., Paris, France). The frictional and wear performance of the films was tested under atmospheric conditions (25% relative humidity) using a ball-disk frictional wear tester (Tribo-S-D-0000, CSM, Basel, Switzerland), and each sample was repeated three times. After the test, the abrasion marks were observed with a three-dimensional surface profiler (MicroXAM-3D, ADE, Santa Barbara, CA, USA), and the wear rate and wear volume were calculated. Volume. The wear spot morphology of the paired balls was observed using an Olympus optical microscope (STM6, Tokyo, Japan). The hardness and elastic recovery properties of the films were characterized using a nanoindenter (NHT2, CSM, Basel, Switzerland) with a nanoindentation loading load of 5 mN and an indentation depth of no more than one-tenth of the film thickness to prevent the influence of the substrate on the test results, and the elastic recovery was calculated using the formula of $(d_{\max} - d_{\min})/d_{\max}$, where d_{\max} and d_{\min} are the maximum and minimum depth of pressure into the film when unloading, respectively. Five points were taken for each sample and tested, and the average value was reported. The acetic acid used in the corrosion test was produced by Leelong Bowa (Tianjin, China) Pharmaceutical Chemicals Co. A UMT-3MT friction tester (UMT-3MT, CETR, Santa Barbara, CA, USA) was used for characterization. Each test for simultaneous performance characterization was repeated three times.

The surface and cross-sectional morphologies of Ti/TiN/a-C:H:Ti films at different titanium target currents are shown in Figure 1. Layer III is a Ti priming layer with a thickness of approximately 0.4 μm , and the presence of the Ti layer enhances the bonding strength between the substrate and the composite film [15]. The cross-sectional structure of the Ti layer can be seen in the figure as a typical columnar crystal structure. Layer II is a TiN transition layer with a thickness of approximately 0.9 μm . It is shown that the transition layer can significantly reduce the residual stress, hinder the crack expansion, and reduce the spalling phenomenon during the friction process, which can well improve the tribological properties of the film [16]. Layer I is a DLC film layer doped with Ti, and the thickness is measured at approximately 1 μm . From the surface morphology, it can be seen that there are particles on the surface of the film. With increasing Ti current, the impurity

particles on the surface of the film gradually decrease, and the surface of the carbon film is smoothest at Ti-2 A. It can be seen in the figure that these films have a uniform structure and good density without obvious defects.

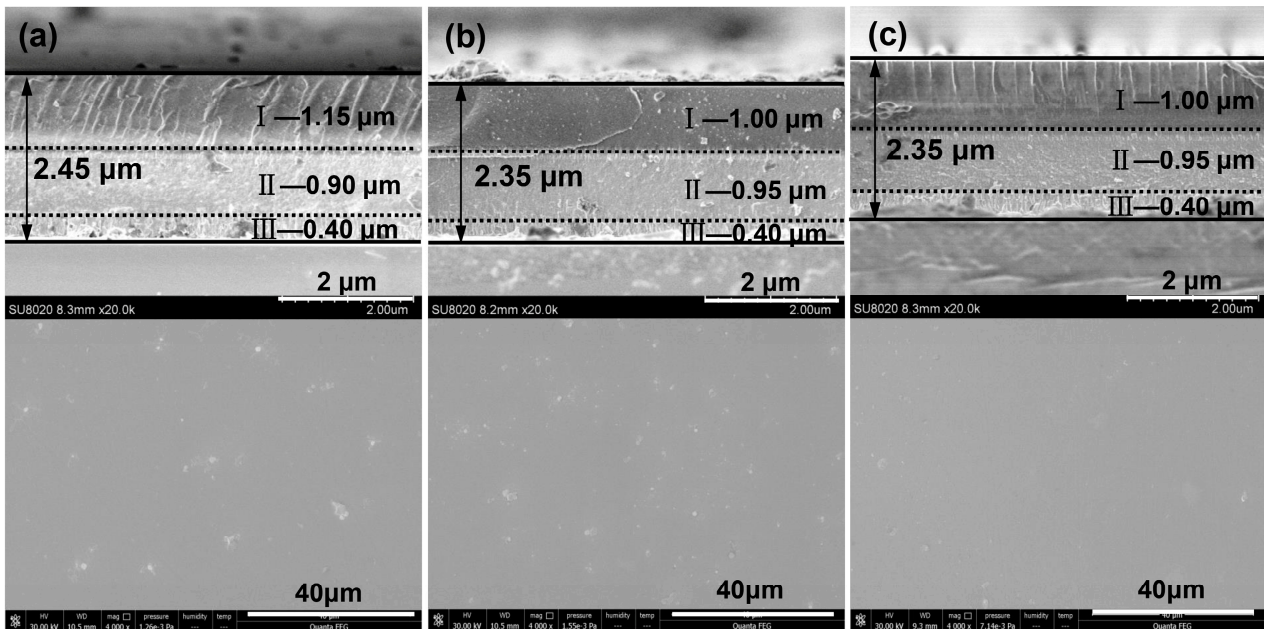


Figure 1. SEM morphology of film cross-section and surface at Ti target sputtering current of (a) Ti-0 A, (b) Ti-1 A, (c) Ti-2 A.

Figure 2a shows the Raman spectra of the films at different titanium currents. The films all exhibit obvious characteristics of diamond-like films, i.e., two peaks, the D peak and the G peak, appear between approximately 1350 cm^{-1} and $1500\text{--}1600\text{ cm}^{-1}$, respectively. Figure 2b shows the variation in the intensity ratio I_D/I_G of the D-peak and G-peak with the titanium current. The ratio of I_D to I_G reaches a minimum when the Ti target sputtering current is 0 A and a maximum when the Ti target sputtering current is 2 A. The intensity ratio of the D-peak to G-peak is related to the content of $\text{sp}^3\text{ C}$ in the film, i.e., the smaller the ratio is, the higher the content of $\text{sp}^3\text{ C}$ [17]. The most important factor determining the mechanical properties of the films is the $\text{sp}^3\text{ C}$ content in the films. The higher the $\text{sp}^3\text{ C}$ content is, the higher the spatial crosslinking of the carbon network composed of it, which gives the films better mechanical properties [18,19]. Compressive stress is the key to the formation of the sp^3 structure, and it can be further speculated that the doping of Ti is better for reducing the internal film stress considering the lower sp^3 content.

Figure 2c shows the nanohardness and elastic modulus of the films for different Ti target currents. The nanohardness of the films decreases from 16.33 GPa to 11.25 GPa, and the elastic modulus decreases from 139.99 GPa to 115.65 GPa with increasing Ti current. The doping of Ti leads to a significant decrease in the hardness of the DLC films on the one hand and improves the bond strength of the film base on the other hand compared with the pure DLC films without doping. This is because the Ti-doped Ti bond easily forms a Ti-C chemical bond with carbon, and the bond energy of the Ti-C bond ($242.52\text{ kJ}\cdot\text{mol}^{-1}$) is smaller than that of the C-C bond in the sp^3 structure ($346\text{ kJ}\cdot\text{mol}^{-1}$). The reduction in hardness of the film [20]. In addition, the sp^3/sp^2 composition ratio in the DLC film structure is very closely related to the hardness, and Ti doping leads to a decrease in the sp^3/sp^2 ratio due to the transition from the sp^3 to the sp^2 structure, thus reducing the hardness of the film [21].

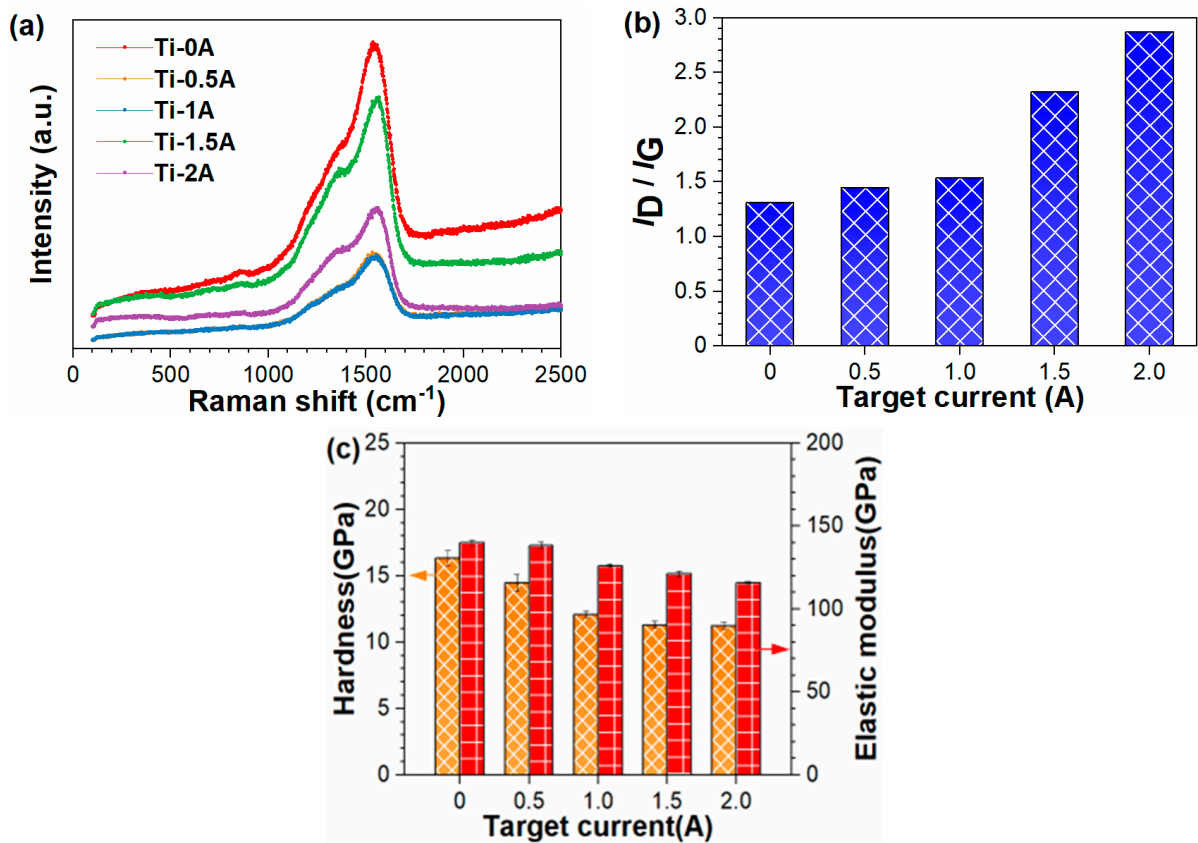


Figure 2. (a) Raman spectrum, (b) intensity ratio of D–peak to G–peak, (c) hardness and elastic modulus of the films at different titanium currents.

Figure 3 shows the scratch optical picture of the bonding strength of the film and substrate. From the figure, we can see that complete peeling of the film occurs at the edge of the scratch, which indicates that the film is well bonded to the substrate. With increasing titanium current, the bonding strength of the film base is gradually enhanced; the lowest bonding strength is 19.54 N for Ti-0 A film, and the best bonding strength is 41.69 N for Ti-2 A film. It is known that an increase in Ti content can enhance the bonding ability of the film and substrate [22].

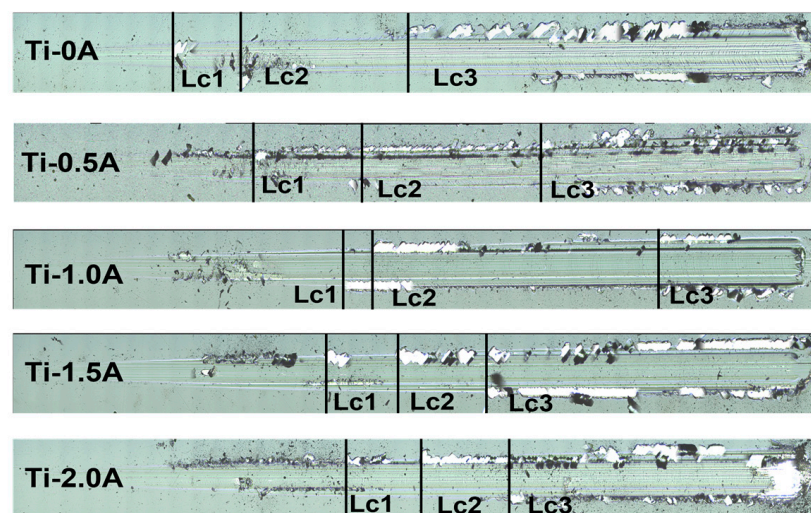


Figure 3. Binding force test diagram of the film under different Ti currents.

Figure 4 shows the friction coefficients of the films under different currents at a 20 N load and the corresponding wear amounts. From Figure 4a, it can be seen that the friction coefficients are high at the initial stage of friction, i.e., the running-in stage, and after a short period of time, the friction coefficients all start to decrease and gradually level off, which is due to the presence of microbump particles on the surface of the film at the initial stage of friction, leading to a high coefficient at the initial stage of friction, and the contact surface of the sample becomes smooth after the friction period. The large particle size on the surface of the Ti-0 A film leads to a large fluctuation of the coefficient throughout the friction period [23]. The friction coefficient gradually decreases as the titanium target current increases, which is due to the doping of Ti causing the film surface to become smooth with fewer microparticles. In Ti-2 A, the shortest distance of the run-in phase is approximately 20 m, and the lowest friction coefficient is approximately 0.028. Figure 4b shows the wear rate and wear volume of the five films, and it can be seen that the wear volume at Ti-0 A, i.e., without element doping, is the largest at approximately $1.85 \times 10^6 \mu\text{m}^3$. With the doping of the elements, it can be seen that the loss volume of the film decreases when the wear volume at Ti-2 A is the smallest at approximately $0.35 \times 10^6 \mu\text{m}^3$.

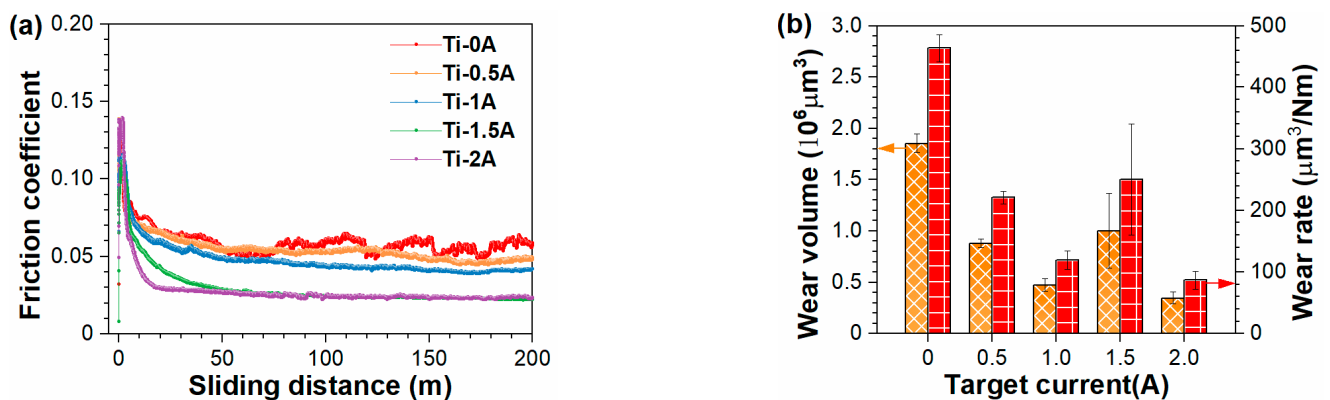


Figure 4. (a) Friction curve and (b) wear volume and wear rate of the film at different titanium currents.

The prepared Ti/TiN/a-C:H:Ti films were subjected to friction tests under atmospheric conditions. As shown in Figure 5, the three-dimensional profile of the abrasion marks shows that the abrasion marks are mainly characterized by furrow wear [24], and the depth of the abrasion marks becomes shallow with increasing Ti current and is lowest at 2 A. From the photomicrographs of the wear spots of the dyadic balls, it can be seen that there are carbon films on the surface of the balls, and the adhesion is slight at the Ti-2 A. Combining the friction coefficient, wear volume, and wear rate, the best tribological performance of the Ti-2 A sample can be seen.

The tribological and mechanical properties of the five prepared DLC films were investigated previously, and it can be seen that the best tribological properties of the films were obtained at Ti-2 A. Therefore, the next step is to study the corrosion and wear properties of the films at Ti-2 A.

As shown in Figure 6a,b show the curves of the friction coefficients of the film and substrate in both solutions with time. It can be observed that the friction coefficients of the film and substrate in both solutions, in the initial phase of friction, are increasing. After a period of friction, the friction interface becomes flat, after which the coefficient of friction gradually reaches a stable value. The difference is that the coefficient of friction of the film has a decreasing trend and then reaches stability, while the coefficient of friction of the substrate increases and then gradually reaches stability [25]. The coefficient of friction of the film in both solutions is lower than that of the substrate. Figure 6c,d shows the wear volume and wear rate of the film and the substrate after friction in both solutions. The wear volume of the film is significantly smaller than that of the substrate, which plays a good protective role. The wear volume of the film and substrate in the acetic acid solution

is higher than that in the aqueous solution due to the higher corrosiveness of the acetic acid solution, which is consistent with the three-dimensional profile and wear depth of the abrasion marks [26].

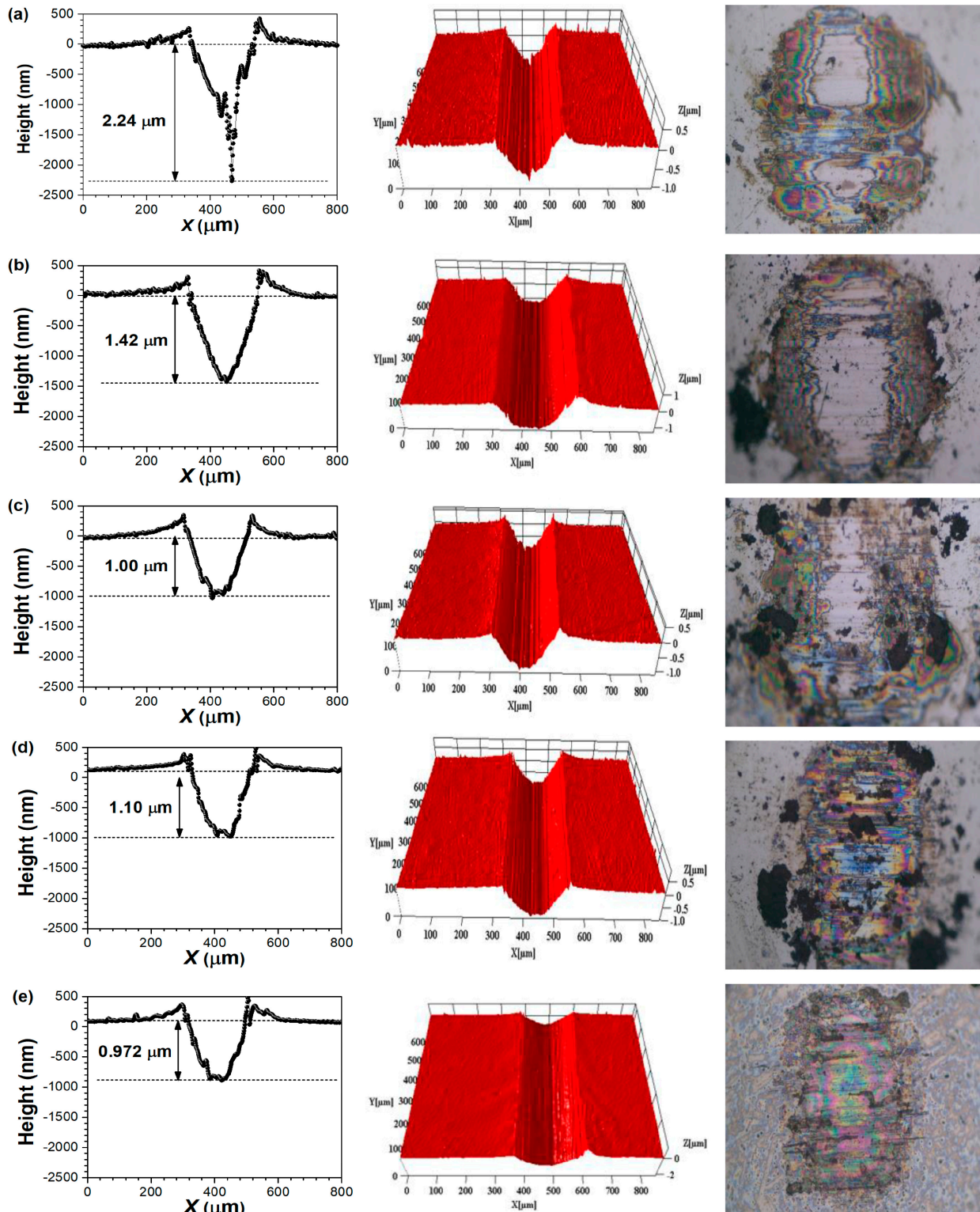


Figure 5. Optical micrographs of abrasion and wear depths, three-dimensional morphology, and dyadic ball wear spots. (a) Ti-0 A, (b) Ti-0.5 A, (c) Ti-1 A, (d) Ti-1.5 A, (e) Ti-2 A.

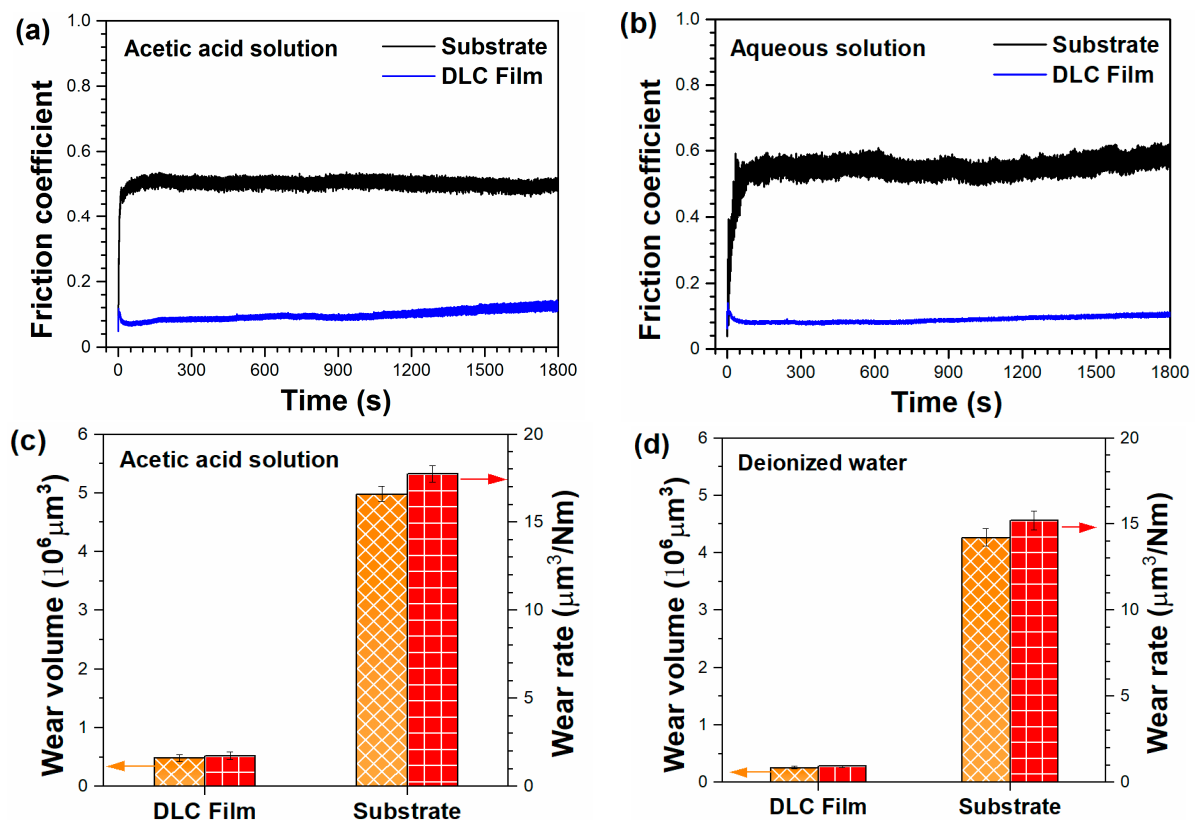
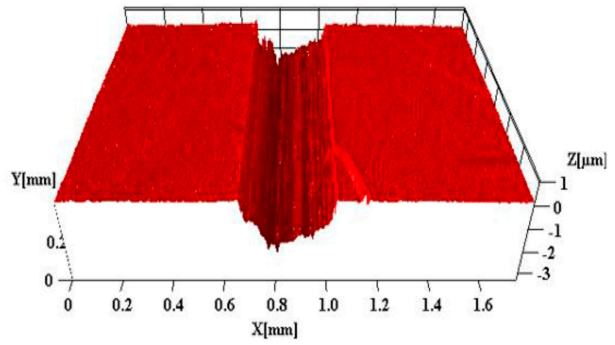
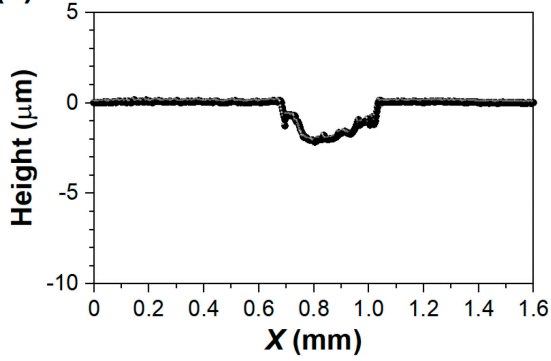


Figure 6. Friction coefficient between Ti-2 A film and substrate: (a) acetic acid solution, (b) aqueous solution and wear volume and wear rate, (c) acetic acid solution, and (d) aqueous solution.

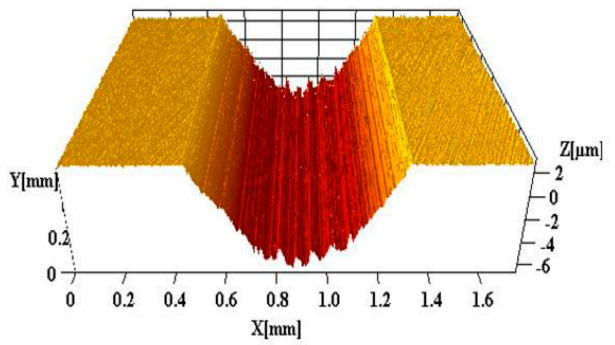
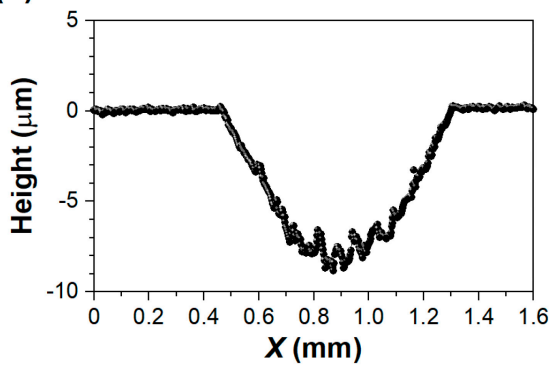
The wear marks and wear depth of the DLC film in both solutions were observed using a three-dimensional profilometer, as shown in Figure 7. It can be observed that the wear marks of the film in both acetic acid solution and aqueous solution are shallower and narrower than those of the substrate, indicating that the DLC film provides good protection to the substrate under corrosive media. The wear depth in the acetic acid solution is deeper than that in the aqueous solution, and it can be seen that the wear depth curve fluctuates more in the acetic acid solution while the wear depth curve is smoother in the aqueous solution because the stronger corrosiveness of the acetic acid solution intensifies the mechanical wear during sliding [27,28].

The open circuit potential tested in a tribocorrosion test is a mixed potential that represents the combined state of worn and unworn material in the wear trajectory. Therefore, it is commonly used to assess the corrosion resistance and stability of the sample [29]. Figure 8a,b show the continuous variation in the open-circuit potential before, during, and after friction for the coated samples and substrates in acetic acid solution (pH = 3) and aqueous solution. The open circuit potential remains stable before the start of friction, which is due to the oxide film generated on the sample surface in the solution, which inhibits the corrosion of the sample by the solution [27,30]. In the initial stage of the friction corrosion test, a sharp decrease in the open circuit potential curve with time was observed due to the change in the contact surface state caused by the sliding of the mating pair on the sample surface. The open-circuit potential stabilized for some time afterwards, which can be explained by the removal and generation of the passivation film reaching a dynamic equilibrium [31,32]. Additionally, the open circuit potential in acidic solution is overall lower than that in aqueous solution, indicating that the film is more prone to corrosion with the substrate in strongly corrosive media. A significant positive shift in the open circuit potential of the film can be seen in the figure, both in the acetic acid solution and in the aqueous solution, indicating that the film has better corrosion resistance than the substrate.

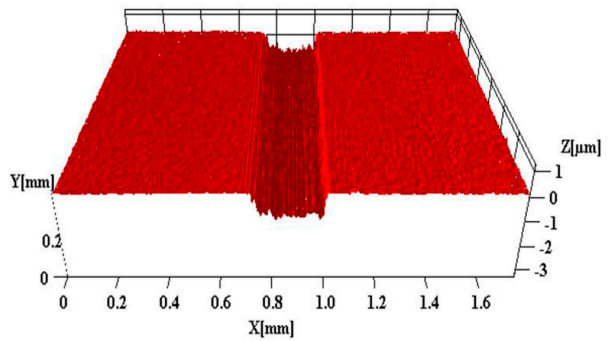
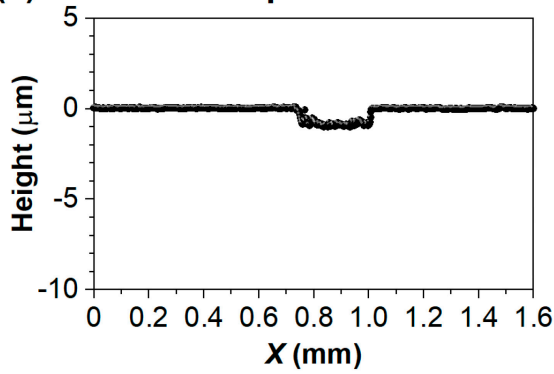
(a) DLC Film in acetic acid solution



(b) Substrate in acetic acid solution



(c) DLC film in aqueous solution



(d) Substrate in aqueous solution

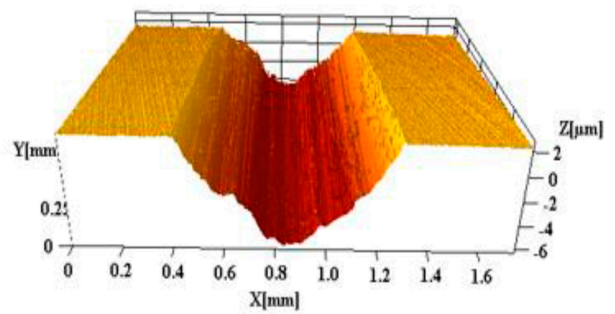
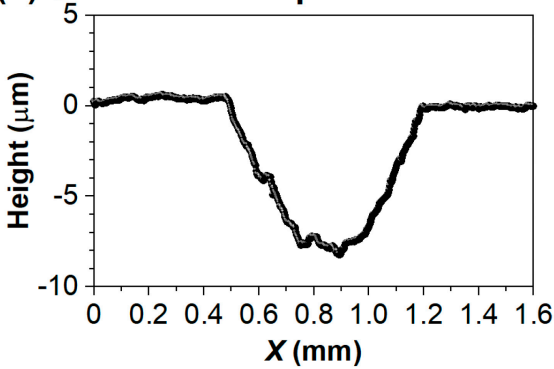


Figure 7. Three-dimensional morphology and wear depth curves of (a) Ti-2 A film and (b) substrate in acetic acid solution and (c) Ti-2 A film and (d) substrate in aqueous solution.

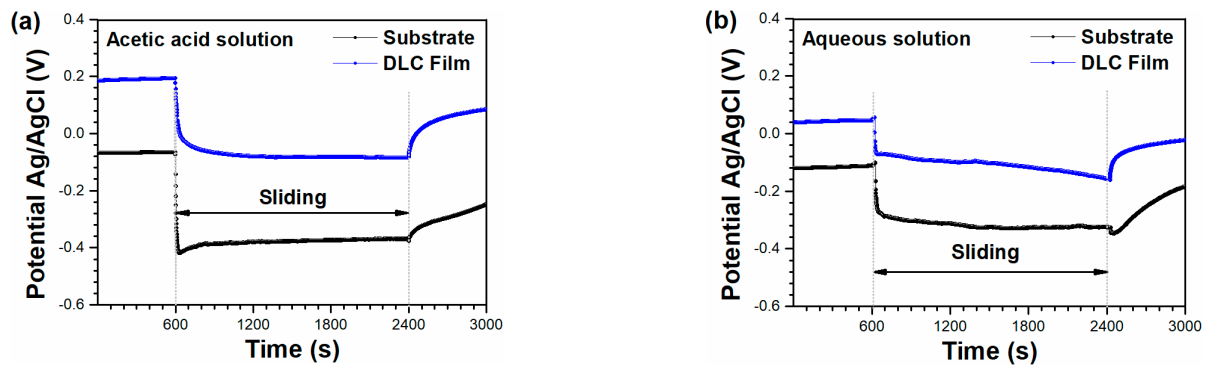


Figure 8. Open circuit potential of film and substrate (a) acetic acid solution (b) aqueous solution.

The Tafel polarization curves of the film and substrate in aqueous solution before, during, and after friction are shown in Figure 9. Table 2 shows the electrochemical parameters of the film and substrate in aqueous solution before, during, and after friction. As seen from the figure, the polarization curve tested before friction had the highest corrosion potential, and the sample was corroded, resulting in a negative shift of the polarization curve due to a change in the state of the contact surface caused by the sliding of the mating sub on the sample surface. The polarization curve after friction was tested a few minutes after the end of friction. The polarization curve shifts positively, but the corrosion potential is still smaller than the potential before friction, which is due to the friction causing the sample surface to be worn down. After the friction ends, the corrosion potential shifts positively due to the generation of a passivation film [33].

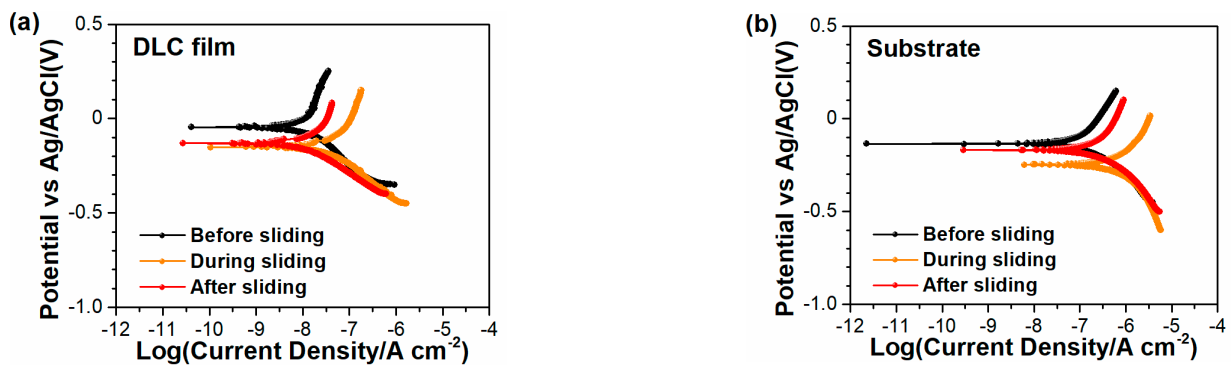


Figure 9. Polarization curves of (a) film and (b) substrate in aqueous solution before, during, and after rubbing.

Table 2. Electrochemical parameters of substrates and films in aqueous solution.

Sample	Before		Sliding		After	
	E_{corr} (V)	I_{corr} (A/cm ²)	E_{corr} (V)	I_{corr} (A/cm ²)	E_{corr} (V)	I_{corr} (A/cm ²)
Ti-2A film	−0.47	6.64×10^{-9}	−0.152	2.35×10^{-8}	−0.170	7.88×10^{-9}
Substrate	−0.137	6.65×10^{-8}	−0.246	4.38×10^{-7}	−0.146	1.46×10^{-7}

The Tafel polarization curves of the film and substrate in acetic acid solution before, during, and after friction are shown in Figure 10. Table 3 shows the electrochemical parameters of the film and substrate in an acetic acid solution before, during, and after friction. The corrosion potential E_{corr} of the film before friction is 0.059 V, and that of the substrate before friction is −0.27 V. When rubbed against the silicon nitride spherical pin, the corrosion potential shifts negatively. The corrosion potential E_{corr} of the film is −0.087 V and the E_{corr} of the substrate is −0.357 V, both of which have different degrees of negative shift,

indicating that mechanical wear can promote electrochemical corrosion of the film and the substrate [34,35]. After the end of the friction due to the sliding stop, the damage to the contact surface of the mating sub stops because the sample surface passivation film generation of corrosion resistance has a slight increase in the corrosion potential for a slight positive shift but does not restore the corrosion potential before the friction [11].

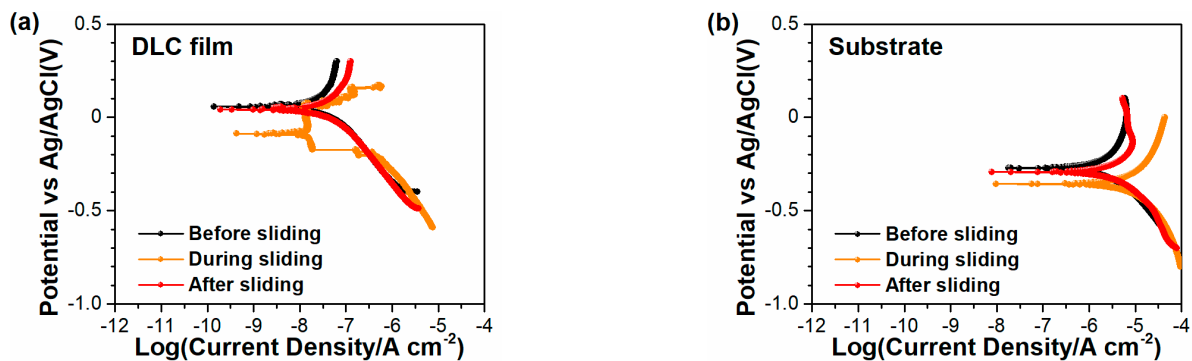


Figure 10. Polarization curves of (a) film and (b) substrate before, during, and after rubbing in acetic acid solution.

Table 3. Electrochemical parameters of substrates and films in acetic acid solution.

Sample	Before		Sliding		After	
	E_{corr} (V)	I_{corr} (A/cm ²)	E_{corr} (V)	I_{corr} (A/cm ²)	E_{corr} (V)	I_{corr} (A/cm ²)
Ti-2A film	0.059	6.607×10^{-9}	-0.087	1.318×10^{-8}	0.042	1.219×10^{-8}
Substrate	-0.270	1.025×10^{-6}	-0.357	5.193×10^{-6}	-0.290	2.692×10^{-6}

3. Conclusions

Ti/TiN/a-C:H:Ti films were prepared using a nonequilibrium magnetron sputtering technique by controlling the titanium target current. The effects of different titanium currents on the film structure, mechanical properties, and tribological properties were investigated. A special focus was paid on the corrosion and wear properties of developed films and their protection performance against metallic substrates in an acetic acid solution with a low pH value of 3.0. The conclusions can be drawn as follows:

- (1) The five films prepared at different sputtering currents on titanium targets were dense in structure and had no other obvious defects. The clustered particles on the surface gradually decreased with the increase in metal element doping content.
- (2) Compared with the undoped film, the bonding between the doped film and the substrate is gradually enhanced as the doping content increases, and the content of sp^2 hybridized carbon in the film is gradually increased, which in turn decreases the friction coefficient.
- (3) The increase in the target current leads to a gradual decrease in the hardness and elastic modulus of the film, which is due to the improved graphitization characterized by the decreasing sp^3 heterocarbon content.
- (4) The developed DLC films improve the corrosion resistance of the metallic substrate in an acetic acid solution with a low pH value of 3.0, although during dynamic wear, the corrosion is accelerated by the continuous wear damage at the surface.
- (5) The prepared multilayer carbon-based films have the potential to be applied as surface protection materials in both wear and corrosive environments.

Author Contributions: Conceptualization, J.L., P.R. and H.L.; methodology, Y.H., X.W. and X.L.; formal Analysis, Y.H., X.W. and C.S.; writing—original draft preparation, Y.H., J.L. and H.L.; supervision, P.R., H.L. and C.S.; visualization, Y.H., X.L. and C.S.; software, Y.H., X.W. and X.L.; writing—review and editing, J.L. and P.R. All authors have read and agreed to the published version of the manuscript.

Funding: The research was supported by the National Key Research and Development Program of China (No. 2021YFB3400400), the National Key Research and Development Program of China (No. 2022YFB3809000), the Fundamental Research Funds for the Central Universities (No. 31920220160), the Youth Innovation Promotion Association of Chinese Academy of Sciences (Y202084), and the Key Program of the Lanzhou Institute of Chemical Physics, CAS (No. KJZLZD-3).

Data Availability Statement: The raw / processed data required to reproduce these findings cannot be shared at this time, as the data also form part of an ongoing study.

Conflicts of Interest: The authors declare no conflict of interest.

References

1. Haibo, S.; Lv, Y.; Huaichao, W.; Limei, Z. Effects of Element Doping on the Structure and Properties of Diamond-like Carbon Films: A Review. *Lubricants* **2023**, *11*, 86.
2. Bociaga, D.; Sobczyk-Guzenda, A.; Szymanski, W.; Jedrzejczak, A.; Jastrzebska, A.; Olejnik, A.; Swiatek, L.; Jastrzebski, K. Diamond like carbon coatings doped by Si fabricated by a multi-target DC-RF magnetron sputtering method—Mechanical properties, chemical analysis and biological evaluation. *Vacuum* **2017**, *143*, 395–406. [[CrossRef](#)]
3. Rajesh Kumar, L.; Amirthagadeswaran, K.S. Corrosion and wear behaviour of nano Al₂O₃ reinforced copper metal matrix composites synthesized by high energy ball milling. *Part. Sci. Technol.* **2019**, *38*, 228–235.
4. Jing, P.P.; Ma, D.L.; Gong, Y.L.; Luo, X.Y.; Zhang, Y.; Weng, Y.J.; Leng, Y.X. Influence of Ag doping on the microstructure, mechanical properties, and adhesion stability of diamond-like carbon films. *Surf. Coat. Technol.* **2021**, *405*, 126542. [[CrossRef](#)]
5. Zhu, L.; Li, J.; Kang, J.; Tang, L.; Ma, G.; Han, C.; Shi, J. Different Cr Contents on the Microstructure and Tribomechanical Properties of Multi-Layered Diamond-Like Carbon Films Prepared by Unbalanced Magnetron Sputtering. *J. Mater. Eng. Perform.* **2020**, *29*, 7131–7140. [[CrossRef](#)]
6. Yukun, Z.; Dongxu, C.; Hongyun, D.; Jilong, Q.; Kaice, Z.; Zhe, L.; Tao, Z.; Peng, G.; Yanwen, Z. DLC (H) coated 13Cr SMSS by high-pulsed power CVD technique. *Surf. Eng.* **2020**, *37*, 1012–1019.
7. Liu, L.; Wu, Z.; An, X.; Shao, T.; Xiao, S.; Cui, S.; Lin, H.; Fu, R.K.Y.; Tian, X.; Chu, P.K.; et al. Improved interfacial adhesion between TiAlN/DLC multi-layered coatings by controlling the morphology via bias. *Surf. Coat. Technol.* **2017**, *331*, 15–20. [[CrossRef](#)]
8. Javidparvar, A.A.; Mosavi, M.A.; Ramezanzadeh, B. Nickel-aluminium bronze (NiBRAI) casting alloy tribological/corrosion resistance properties improvement via deposition of a Cu-doped diamond-like carbon (DLC) thin film; optimization of sputtering magnetron process conditions. *Mater. Chem. Phys.* **2023**, *296*, 127279. [[CrossRef](#)]
9. Su, Y.; Huang, W.; Cai, L.; Gong, X.; Zhang, T.; Hu, R.; Zhang, P.; Ruan, H. Microstructural evolution and tribology of Mo-doped diamond like carbon nanocomposite film. *Tribol. Int.* **2022**, *174*, 107774. [[CrossRef](#)]
10. Zhang, S.; Yan, M.; Yang, Y.; Zhang, Y.; Yan, F.; Li, H. Excellent mechanical, tribological and anti-corrosive performance of novel Ti-DLC nanocomposite thin films prepared via magnetron sputtering method. *Carbon* **2019**, *151*, 136–147. [[CrossRef](#)]
11. Li, L.; Liu, L.-L.; Li, X.; Guo, P.; Ke, P.; Wang, A. Enhanced Tribocorrosion Performance of Cr/GLC Multilayered Films for Marine Protective Application. *ACS Appl. Mater. Interfaces* **2018**, *10*, 13187–13198. [[CrossRef](#)]
12. Saad, M.F.; Dongxu, C.; Shengli, L.; Yanwen, Z.; Hongbin, W.; Sadawy, M.M. Corrosion behavior and passive stability of multilayer DLC-Si coatings. *Surf. Coat. Technol.* **2021**, *431*, 128001.
13. Baorui, S.; Yong, H.; Chaozheng, Z.; Yanhuai, L.; Liuquan, Y.; Zhongxiao, S. Fabrication and anticorrosion behavior of a bi-phase TaNbHfZr/CoCrNi multilayer coating through magnetron sputtering. *Corros. Sci.* **2021**, *196*, 110020.
14. Ye, Y.; Wang, Y.; Ma, X.; Zhang, D.; Wang, L.; Li, X. Tribocorrosion behaviors of multilayer PVD DLC coated 304L stainless steel in seawater. *Diam. Relat. Mater.* **2017**, *79*, 70–78. [[CrossRef](#)]
15. Cao, H.; Qi, F.; Ouyang, X.; Zhao, N.; Zhou, Y.; Li, B.; Luo, W.; Liao, B.; Luo, J. Effect of Ti Transition Layer Thickness on the Structure, Mechanical and Adhesion Properties of Ti-DLC Coatings on Aluminum Alloys. *Materials* **2018**, *11*, 1742. [[CrossRef](#)]
16. Wei, J.; Li, H.; Liu, L.; Guo, P.; Ke, P.; Wang, A. Enhanced tribological and corrosion properties of multilayer ta-C films via alternating sp³ content. *Surf. Coat. Technol.* **2019**, *374*, 317–326. [[CrossRef](#)]
17. Sun, J.; Tang, Y.; Xu, X.; Li, Z.; Su, F. Synthesis of Nitrogen-Doped Diamond-Like Carbon Films Produced by Plasma-Enhanced Chemical Vapor Deposition and their Tribocorrosion Behavior in Hanks' Solution. *J. Mater. Eng. Perform.* **2022**, *31*, 8334–8345. [[CrossRef](#)]
18. Wang, Y.; Li, H.; Ji, L.; Zhao, F.; Li, J.; Liu, X.; Wu, Y.; Lv, Y.; Fu, Y.; Zhou, H.; et al. Study on the microstructure and properties of graphite-like carbon films deposited by unbalanced magnetron sputtering. *Proc. Inst. Mech. Eng. Part J J. Eng. Tribol.* **2012**, *226*, 714–721. [[CrossRef](#)]

19. Ahmad, K.; Hassan, E.; Masoud, A.; Amir, M. Modified diamond-like carbon (Cr-DLC) coating applied by PACVD-CAPVD hybrid method: Characterization and evaluation of tribological and corrosion behavior. *Diam. Relat. Mater.* **2023**, *136*, 109968.
20. Nie, C.; Chang, B.; Xie, H. Structure analysis of Ti doped DLC coatings deposited by unbalanced magnetron sputtering. *Acta Metall. Sin.* **2007**, *43*, 1207–1210.
21. Bootkul, D.; Saenphinit, N.; Supsermpol, B.; Aramwit, C.; Intarasiri, S. Synthesis of Ti-doped DLC film on SS304 steels by Filtered Cathodic Vacuum Arc (FCVA) technique for tribological improvement. *Appl. Surf. Sci.* **2014**, *310*, 293–299. [[CrossRef](#)]
22. Martin, Z.; Volker, W.; Jörg, K.; Martina, Z. Effect of doping elements to hydrogen-free amorphous carbon coatings on structure and mechanical properties with special focus on crack resistance. *Mater. Sci. Eng. A* **2022**, *857*, 144086.
23. Xiang, D.; Zhang, Z.; Chen, Y.; Hu, Y.; Lei, X. Study of Tribological Properties of Textured Boron-Doped Diamond Film under Water Lubrication. *Surf. Interfaces* **2021**, *23*, 100983. [[CrossRef](#)]
24. Yanchao, Z.; Feng, X.; Dan, Z.; Ji, X.; Xianqing, S.; Shuo, S.; Wenxuan, Z.; Chengzuan, G.; Dunwen, Z. Enhanced tribological and corrosion properties of DLC/CrN multilayer films deposited by HPPMS. *Ceram. Int.* **2022**, *48*, 25569–25577.
25. Chen, H.; Zhang, G.; Lu, Z.; Bai, L. Frictional behaviors of diamond-like carbon films under water lubrication: A molecular dynamics study. *Tribol. Int.* **2021**, *153*, 106609. [[CrossRef](#)]
26. Wu, J.; Chen, L.; Ning, C.; Wu, G.; Lu, Z.; Shang, L.; Wu, Z.; Zhang, G. Tribo-mechanism of amorphous carbon films under corrosion solution and various mechanical loads. *Diam. Relat. Mater.* **2021**, *114*, 108318. [[CrossRef](#)]
27. Shang, L.; Gou, C.; Li, W.; He, D.; Wang, S. Effect of microstructure and mechanical properties on the tribological and electrochemical performances of Si/DLC films under HCl corrosive environment. *Diam. Relat. Mater.* **2021**, *116*, 108385. [[CrossRef](#)]
28. Xu, X.; Guo, P.; Zuo, X.; Sun, L.; Li, X.; Lee, K.-R.; Wang, A. Understanding the effect of Al/Ti ratio on the tribocorrosion performance of Al/Ti co-doped diamond-like carbon films for marine applications. *Surf. Coat. Technol.* **2020**, *402*, 126347. [[CrossRef](#)]
29. Jianzhuo, G.; Ningxi, W.; Hui, C.; Xuexu, X. The Influence of 1 wt.% Cr on the Corrosion Resistance of Low-Alloy Steel in Marine Environments. *Metals* **2023**, *13*, 1050.
30. Wen, X.; Zhong, Y.; Lele, L.; Moucheng, L. Electrochemical Corrosion Behavior of 310S Stainless Steel in Hot Concentrated Tap Water. *Metals* **2023**, *13*, 713.
31. Yuhua, Z.; Jianzhang, W.; Hao, L.; Fengyuan, Y. The Tribo-Corrosion Behavior of Monel 400 Alloy in Marine Environment at Varied Rotational Velocities. *Metals* **2022**, *12*, 1503.
32. Yuhua, Z.; Hao, L.; Dongyue, Z.; Jianzhang, W.; Fengyuan, Y. Effect of polarization potentials on tribocorrosion behavior of Monel 400 alloy in seawater environment. *Tribol. Int.* **2022**, *168*, 107445.
33. Abdelkarim Ait, M.; Badr, E.-H.; Raihana Jannat, A.; Hassane, L.; Rachid, S.; Hanseung, L.; Mustafa, R.A.; Mouslim, M.; Khadija, H.; Ismat, H.A. Insights into the Corrosion Inhibition Performance of Isonicotinohydrazide Derivatives for N80 Steel in 15% HCl Medium: An Experimental and Molecular Level Characterization. *Metals* **2023**, *13*, 797.
34. Zhang, P.; Shan, L.; Su, X.; Huang, Z.; Luo, L.; Chen, J. Microstructure and tribological performance of CrTiSiCN coatings on 316L and TC4 in seawater. *Tribol. Int.* **2021**, *156*, 106832. [[CrossRef](#)]
35. Wang, C.; Sui, X.; Lu, X.; Zhang, X.; Yan, Z.; Lu, Y.; Hao, J. Friction and wear of a-C:H films deposited at different bias in air and NaCl solution. *Tribol. Int.* **2022**, *175*, 107863. [[CrossRef](#)]

Disclaimer/Publisher's Note: The statements, opinions and data contained in all publications are solely those of the individual author(s) and contributor(s) and not of MDPI and/or the editor(s). MDPI and/or the editor(s) disclaim responsibility for any injury to people or property resulting from any ideas, methods, instructions or products referred to in the content.